ECCENTRIC COMPRESSIVE STRENGTH OF HIGH STRENGTH STEEL OCTAGONAL TUBE STUB COLUMNS

HAN FANG[1], TAK-MING CHAN[2] and BEN YOUNG[3]

[1] School of Civil, Environmental and Mining Engineering, The University of Adelaide, SA 5005, Australia (Formerly, Department of Civil and Environmental Engineering, The Hong Kong Polytechnic University, Hong Kong, China)
E-mail: han.fang@adelaide.edu.au
[2] Department of Civil and Environmental Engineering, The Hong Kong Polytechnic University, Hong Kong, China.
E-mail: tak-ming.chan@polyu.edu.hk
[3] Department of Civil and Environmental Engineering, The Hong Kong Polytechnic University, Hong Kong, China (Formerly, Department of Civil Engineering, The University of Hong Kong, Pokfulam Road, Hong Kong, China)
E-mail: ben.young@polyu.edu.hk

An experimental investigation into the behavior of high strength steel (HSS) octagonal tube stub columns subject to combined compression and bending is presented in this paper. HSS octagonal tube stub column specimens fabricated using S690 steel plates with a nominal yield strength of 690MPa were prepared. The measurements of material properties and initial local geometric imperfections for the specimens were carried out and the results are reported. The experimental set-up and testing procedures for the specimens subject to various combinations of compression and bending are presented in this paper. The load-deformation behavior, ultimate loads and failure modes of the specimens are also discussed. A finite element (FE) model for the HSS octagonal tube stub columns under combined compression and bending was also developed and the FE model was validated against the results from experiments. The FE model can be applied to predict the behavior of HSS octagonal tube stub columns subject to combined compression and bending for structural designs.

Keywords: High strength steel; Octagonal tube stub columns; Experiments; Combined compression and bending; Finite element modeling.

1 Introduction

High strength steel (HSS) with nominal yield strength over 460MPa and up to 1100MPa has been available to be used as construction materials for various structural applications (Ma et al. 2015, Fang et al. 2018a). The usage of HSS allows to reduce the structural element sizes and subsequently brings the benefits of savings of weight consumption of construction materials, easier handling for construction and lower structural embodied carbon-footprint. In order to safely design HSS structures, numerous studies have been conducted on HSS structures with I-section, circular hollow sections and rectangular hollow sections and investigated the behavior of these structures subject to compression (Ma et al. 2016, Ban et al. 2018, Fang et al. 2018a, Li et al. 2019), bending (Wang et al. 2016, Ma et al. 2017) and combined compression and bending

Proceedings of the 17th International Symposium on Tubular Structures.
Editors: X.D. Qian and Y.S. Choo

Published by Research Publishing, Singapore.
ISBN: 978-981-11-0745-0; doi:10.3850/978-981-11-0745-0_063-cd

(Ma et al. 2017, Ma et al. 2018). Although these systematic studies have been conducted on HSS structures with different cross-section shapes, much less attention has been paid to the HSS structures with octagonal hollow sections which demonstrate higher local buckling resistance than structures with I-section or rectangular hollow sections and allow easier connection generation (Bulson 1969, Hassanein et al. 2017). In order to clearly understand the behavior of HSS structures with octagonal hollow sections, Fang and co-researchers investigated the properties and residual stresses of HSS octagonal hollow sections (Fang et al. 2018b) and examined the local buckling behavior of the HSS octagonal hollow section stub columns under axial compression (Fang et al. 2018c). However, no clear understanding on the behavior of the HSS octagonal hollow section stub columns under eccentric compression has been obtained.

Therefore, the current study is carried out to examine the behavior of the stub columns under eccentric compression. HSS octagonal hollow section stub column specimens were prepared. These specimens were tested under eccentric compression with different initial loading eccentricities. Ultimate loads, load-deformation behavior and failure modes of the specimens were obtained and presented. A finite element model was also developed and validated using the results obtained from the eccentric compression tests for investigating the behavior of HSS octagonal hollow section stub columns under eccentric compression.

2 Experimental Investigations

2.1 *Specimens*

Octagonal hollow section stub column specimens were fabricated using S690 steel plates with a nominal yield strength of 690MPa and a thickness of 6mm. During the fabrication process, steel plates were firstly made into half-sections through press-braking and two half-sections were welded to form an octagonal hollow section specimen, as shown in Figure 1. For the specimens, two nominal cross-sectional dimensions were used. For each dimension, three specimens were prepared to be tested under axial compression and eccentric compression with two nominal initial loading eccentricities (e) of 25 and 50mm. The labels and measurement results of dimensions for the specimens are shown in Table 1. In the table, the specimens are labelled based on a nominal cross-sectional dimensions and nominal e values. For example, the label "OHS-70*6-e25" refers to the octagonal hollow section stub column specimen with a nominal edge length (B) and plate thickness (t) of 70 and 6mm respectively and loaded with the e of 25mm. After the measurements of dimensions for the specimens, each specimen was milled flat on both ends which were subsequently welded to end plates of 25mm in thickness.

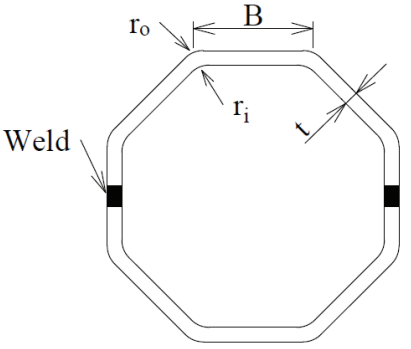

Figure 1. A schematic view of an octagonal hollow section.

Table 1. Dimensions of specimens and loading eccentricities.

Specimen	B (mm)	t (mm)	Length L (mm)
OHS-50*6-e0	50.2	5.95	231.3
OHS-50*6-e25	49.7	5.95	230.0
OHS-50*6-e50	48.9	5.90	228.1
OHS-70*6-e0	69.5	5.88	358.0
OHS-70*6-e25	70.1	6.00	358.6
OHS-70*6-e50	70.4	5.90	359.3

2.2 *Geometric imperfections*

Geometric imperfections exist in the octagonal hollow sections due to fabrication processes and can affect the structural behavior. Due to the relatively short length of the stub column specimens, local geometric imperfections can influence the structural behavior while the influence of global geometric imperfections is relatively insignificant (Ma et al. 2017, Zhao et al. 2016). Therefore, local geometric imperfections were measured for HSS octagonal hollow section stub columns and the results were reported in Fang et al. (2019). A model given as Eq. (1) below was reported in Fang et al. (2019) for estimating the maximum local geometric imperfections ($\omega_{D\&W}$) for the HSS octagonal hollow sections. In the equation, $\sigma_{0.2}$ is the 0.2% proof stress while f_{cr} is the elastic buckling stress for the plate with the highest slenderness in a cross-section (Dawson and Walker 1972).

$$\omega_{D\&W}=0.307*(\sigma_{0.2}/f_{cr})^{0.5}*t \quad (1)$$

2.3 *Test set-up and procedures*

The specimens were tested under axial compression or eccentric compression using an Instron hydraulic testing machine with a capacity of 5000kN. The test set-up is shown in Figure 2. As can be seen in the figure, each specimen was bolted with the wedge plates and its location was adjusted to obtain its specific e value. The two parallel knife edges shown in Figure 2 provide pinned boundary conditions for each specimen. Three displacement transducers were applied to measure the axial shortening and end-rotations of each specimen. Another transducer was also used to measure the mid-height deflection. An initial load of about 3kN was applied to ensure the full contact between different components in the set-up. Before the commencement of each test, the initial e value for each specimen was carefully measured using a theodolite by comparing the space coordinates of the center point marked on the front face of the specimen with those of the front center of the knife edges. The measured initial e values are presented in Table 2. Upon the measurements of the e value, loading was subsequently applied through the displacement-control at a rate of 0.3mm/min and paused for 90 seconds near the ultimate load to obtain the static responses of each specimen (Fang et al. 2018c and 2019).

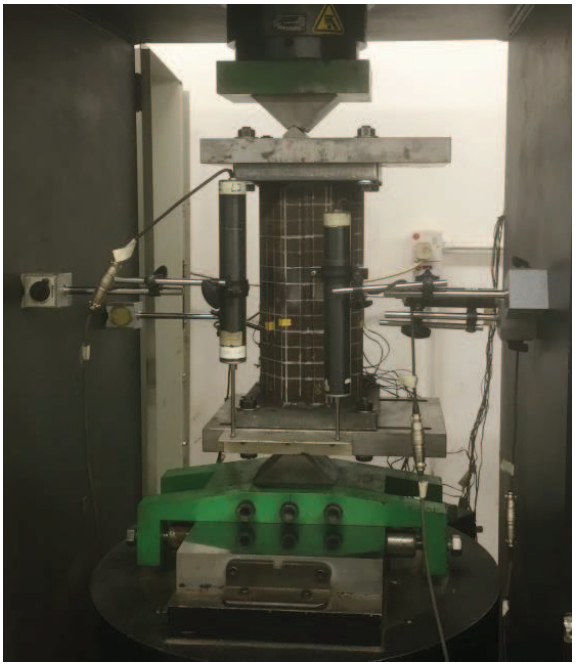

Figure 2. Test set-up.

Table 2. Test results for HSS octagonal tubular stub columns under concentric and eccentric compression.

Specimen	e (mm)	$N_{u,test}$ (kN)	$M_{u,test}$ (kNm)	$N_{u,FE}$ (kN)	$M_{u,FE}$ (kNm)	$N_{u,FE}/N_{u,test}$	$M_{u,FE}/M_{u,test}$
OHS-50*6-e0	-0.04	1778.5	6.8	1765.3	6.6	0.99	0.97
OHS-50*6-e25	25.15	1177.1	33.0	1180.6	33.2	1.00	1.01
OHS-50*6-e50	51.26	843.2	45.9	861.9	46.5	1.02	1.01
OHS-70*6-e0	0.33	2420.5	7.3	2445.1	7.2	1.01	0.99
OHS-70*6-e25	25.77	1818.3	52.4	1826.9	51.2	1.00	0.98
OHS-70*6-e50	49.94	1441.7	77.6	1428.6	77.5	0.99	1.00
					Mean	1.00	0.99
					COV	0.01	0.02

2.4 *Test results*

Experimental results of ultimate load ($N_{u,test}$), ultimate moment ($M_{u,test}$) and load-deformation responses were obtained. The ultimate load ($N_{u,test}$) and ultimate moment ($M_{u,test}$) results for the specimens are provided in Table 2. The $M_{u,test}$ for each specimen was estimated based on the $N_{u,test}$, e value and corresponding mid-height deflection measured at $N_{u,test}$ during the test. Typical load-end rotation curves are also presented in Figures 3 and 4 for OHS-50*6-e25 and OHS-70*6-e50 specimens respectively while failure modes for these specimens are given in Figures 5 and 6.

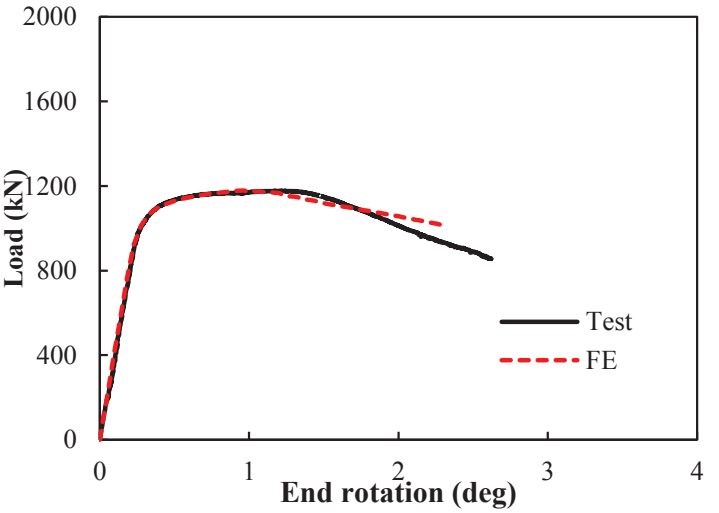

Figure 3. Load-end rotation curve of OHS-50*6-e25 specimen.

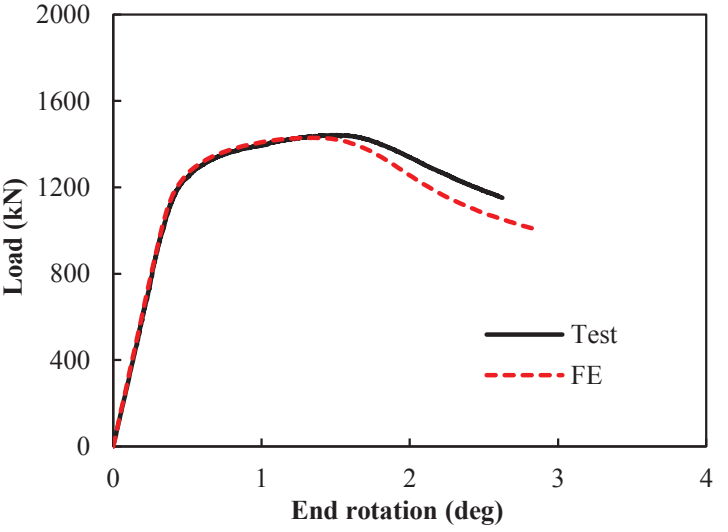

Figure 4. Load-end rotation curve of OHS-70*6-e50 specimen.

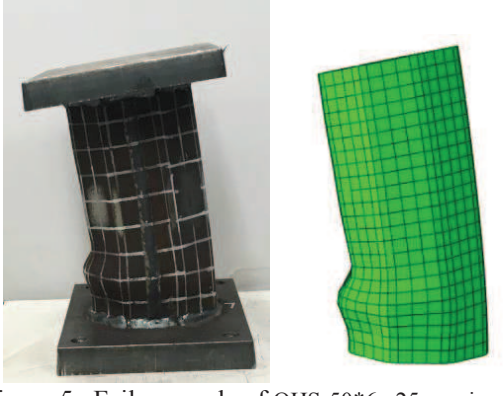

Figure 5. Failure mode of OHS-50*6-e25 specimen.

Figure 6. Failure mode of OHS-70*6-e50 specimen.

3 Finite Element Modeling

3.1 *Finite element model*

Finite element (FE) modeling using the software package ABAQUS 6.14 was also conducted, aiming to develop the FE model with the capability of replicating the test results presented in Section 2.4 and to apply the FE model for predicting the behavior of HSS octagonal hollow section stub columns subject to eccentric compression for structural design and analysis purposes. The four-noded shell element, S4R, with reduced integration was selected for the modeling. A mesh seed size of 10mm was used based on mesh sensitivity studies. Material properties are required as input for FE modeling. Static material properties and stress-strain curves for both flat and corner regions of HSS octagonal hollow sections were measured and reported in Fang et al. (2018b) and a stress-strain model was also proposed in the study for estimating the stress-strain relationship for the materials across HSS octagonal hollow sections. The stress-strain curves estimated using the model based on the average measured properties for different HSS octagonal hollow sections in the study of Fang et al. (2018b) were adopted for the FE modeling in the current study. The obtained stress-strain curves for the flat and corner regions were converted into the true stress-log plastic strain curves using the following equations and these true stress-log plastic strain curves were incorporated in the modeling. In Eqs. (2) and (3), in which ε_{ln}^{pl} is the logarithmic plastic strain, E is the Young's modulus, σ_{true} is the true stress, ε and σ respectively are the engineering strain and engineering stress from the stress-strain curves estimated using the model given by Fang et al. (2018b).

$$\sigma_{true}=\sigma\ (1+\varepsilon) \tag{2}$$

$$\varepsilon_{ln}^{pl}=\ln(1+\varepsilon)-\sigma/E \tag{3}$$

Residual stresses were also found in HSS octagonal hollow sections due to the press-braking and welding fabrication processes and can influence the structural behavior. The distribution and magnitudes of longitudinal bending and membrane residual stresses across HSS octagonal hollow sections was investigated by Fang et al. (2018b). The longitudinal bending residual stresses were inherently incorporated in the material properties as input in the model since the material properties were obtained using the coupon specimens extracted from the HSS octagonal hollow sections (Fang et al. 2018b, Ma et al. 2017). The longitudinal membrane

residual stresses were estimated using the model proposed by Fang et al. (2018b) for the stub columns and included in the FE model.

Initial geometric imperfections can also affect the structural behavior of HSS octagonal hollow sections (Fang et al. 2018c, 2019). Local geometric imperfections were incorporated in the FE model in the form of lowest local buckling mode shape obtained by conducting prior elastic eigenvalue buckling analysis, with the amplitudes estimated from Eq. (1). Boundary conditions were also arranged using two reference points. For each HSS octagonal hollow section stub column, the reference points were offset from the centroid of the cross-section by the e value applied in the corresponding test. Each reference point was coupled with the end nodes on one side of the structure. At the reference point on the unloaded side, the translation was restrained while the rotation about the buckling axis was allowed. The same boundary condition was also applied to the reference point on the loaded side except that the longitudinal translation was allowed. Loading was applied at the reference point located at the loaded side by specifying the displacement in the longitudinal direction in a Riks step which was adopted to predict the ultimate loads and load-displacement responses for the HSS octagonal hollow stub columns.

3.2 *Validation*

The FE model described in the previous section was validated against the test results presented in Section 2.4. The ultimate loads ($N_{u,FE}$) and ultimate moment ($M_{u,FE}$) estimated in the FE modeling were first compared with the test results, as shown in Table 2. The $N_{u,FE}$ values agree well with the $N_{u,test}$ from the tests with the mean $N_{u,FE}/N_{u,test}$ ratio of 1.0 and coefficient of variation (COV) of 0.01. The $M_{u,FE}$ values also compared well with the $M_{u,test}$ values from experiments with the mean $M_{u,FE}/M_{u,test}$ ratio of 0.99 and coefficient of variation (COV) of 0.02. Load-end rotation curves estimated in FE modeling for OHS-50*6-e25 and OHS-70*6-e50 specimens were also found to compare well with the test results, as shown in Figs. 3 and 4. Failure modes predicted in modeling are also presented in Figs. 5 and 6 in comparison with the test results. It can be seen in the figures that the failure modes were accurately predicted by the FE modeling. These comparisons between the results from FE modeling and those test results demonstrate that the FE model can replicate the test results. Thus, the model can be applied to investigate the behavior of HSS octagonal hollow section stub columns subject to eccentric compression.

4 Conclusions

Behavior of HSS octagonal hollow section stub columns under eccentric compression was investigated experimentally and numerically. Six stub column specimens fabricated using S690 steel plates were prepared, covering two nominal cross-section sizes with different plate width-to-thickness ratios. These specimens were tested under axial compression and eccentric compression with different initial loading eccentricities. The test results show that the ultimate loads of the specimens decrease with increasing loading eccentricities. Nonlinear finite element (FE) model was also developed and validated to be capable of accurately predicting the test results of ultimate loads, load-displacement responses and failure modes of the HSS octagonal hollow section stub columns. Therefore, the FE model can be applied to conduct accurate modeling to predict the behavior of HSS octagonal hollow section stub columns under eccentric compression.

Acknowledgements

The research work described in this paper was supported by a grant from the Research Grants Council of the Hong Kong Special Administrative Region, China (Project no. 15218918).

References

Bulson, P.S., The strength of thin-walled tubes formed from flat elements, *Int. J. Mech. Sci.,* 11, 613-25, Jan, 1969.

Ban, H.Y. and Shi, G., Overall buckling behaviour and design of high-strength steel welded section columns, *J. Constr. Steel Res.*, 143, 180-195, 2018.

Dawson, R.G. and Walker, A.C., Post-buckling of geometrically imperfect plates, *J. Struct. Div.*, 98, 75-94, 1972.

Fang, H., Chan, T.M. and Young, B., Structural performance of cold-formed high strength steel tubular columns, *Eng. Struct.*, 177, 473-488, 2018a.

Fang, H., Chan, T.M. and Young, B., Material properties and residual stresses of octagonal high strength steel hollow sections, *J. Constr. Steel Res.*, 148, 479-490, 2018b.

Fang, H., Chan, T.M. and Young, B., Behaviour of S690 steel fabricated octagonal shaped hollow stub columns, in Proceedings of the 8th International Conference on Thin-Walled Structures, Lisbon, Portugal, 2018c.

Fang, H., Chan, T.M. and Young, B., Behavior of octagonal high strength steel tubular stub columns, *J. Struct. Eng.*, 2019. (In press)

Hassanein, M.F., Patel, V.I., Elchalakani, M. and Thai, H.T., Finite element analysis of large diameter high strength octagonal CFST short columns, *Eng. Struct.*, 30, 473-488, 2018.

Li, D.X., Huang, Z.C., Uy, B., Thai, H.T. and Hou, C., Slenderness limits for fabricated S960 ultra-high-strength steel and composite columns, *J. Constr. Steel Res.*, 159, 109-121, 2019.

Ma, J.L., Chan, T.M. and Young, B., Material properties and residual stresses of cold-formed high strength steel hollow sections, *J. Constr. Steel Res.*, 109, 152-165, 2015.

Ma, J.L., Chan, T.M. and Young, B., Experimental investigation on stub-column behavior of cold-formed high-strength steel tubular sections, *J. Struct. Eng.*, 142(5), 04015174, 2016.

Ma, J.L., Chan, T.M. and Young, B., Design of cold-formed high strength steel tubular beams, *Eng. Struct.*, 151, 432-443, 2017.

Ma, J.L., Chan, T.M. and Young, B., Experimental investigation on cold-formed high strength steel circular hollow sections under combined compression and bending, *in Proceedings of Eurosteel*, 3622-3630, 2017.

Ma, T.Y., Li, G.Q. and Chung, K.F., Numerical investigation into high strength Q690 steel columns of welded H-sections under combined compression and bending, *J. Constr. Steel Res.*, 144, 119-134, 2018.

Wang, J., Afshan, S., Gkantou, M., Theofanous, M., Baniotopoulos, C. and Gardner, L., Flexural behaviour of hot-finished high strength steel square and rectangular hollow sections, *J. Constr. Steel Res.*, 121, 97-109, 2016.

Zhao, O., Rossi, B., Gardner, L. and Young, B., Experimental and numerical studies of ferritic stainless steel tubular cross sections under combined compression and bending, *J. Struct. Eng.*, 142, 04015110, 2016.